CO2 Capture by Hydroxylated Azine-Based Covalent Organic Frameworks

Renata Avena Maia, Felipe Lopes Oliveira, Vincent Ritleng, Qiang Wang, Benoît Louis, Pierre Mothé Esteves

CO_2 Capture by Hydroxylated Azine-Based Covalent Organic Frameworks

Renata Avena Maia,[a,b] Felipe Lopes Oliveira,[a] Vincent Ritleng,[c] Qiang Wang,[d] Benoît Louis,*[b] Pierre Mothé Esteves* [a]

[a] Dr. R. A. Maia, M.Sc. F. L. Oliveira, Prof. P. M. Esteves
Instituto de Química
Universidade Federal do Rio de Janeiro
Av. Athos da Silveira Ramos, 149, CT, Bl. A-622, Cid. Universitária, Ilha do Fundão, Rio de Janeiro, RJ, 21941-909, Brazil.
E-mail: pesteves@iq.ufrj.br

[b] Dr. R. A. Maia, Dr. B. Louis
Université de Strasbourg
CNRS, ICPEES, UMR 7515, 25 rue Becquerel, 67087 Strasbourg, France.
E-mail: blouis@unistra.fr

[c] Prof. V. Ritleng
Université de Strasbourg
CNRS, LIMA, UMR 7042, 25 rue Becquerel, 67087 Strasbourg, France.

[d] Prof. Q. Wang
College of Environmental Science and Engineering
Beijing Forestry University
35 Qinghua E Rd, Haidian District, Beijing 100083, China.

Supporting information for this article is given via a link at the end of the document.

Abstract: Covalent Organic Frameworks RIO-13, RIO-12, RIO-11, and RIO-11m were investigated towards their CO_2 capture properties by thermogravimetric analysis at 1 atm and 40 °C. These microporous COFs bear in common the azine backbone composed of hydroxy-benzene moieties but differ in the relative number of hydroxyl groups present in each material. Thus, their sorption capacities were studied as a function of their textural and chemical properties. Their maximum CO_2 uptake values showed a strong correlation with an increasing specific surface area, but that property alone could not fully explain the CO_2 uptake data. Hence, the specific CO_2 uptake, combined with DFT calculations, indicated that the relative number of hydroxyl groups in the COF backbone acts as an adsorption threshold, as the hydroxyl groups were indeed identified as relevant adsorption sites in all the studied COFs. Additionally, the best performing COF was thoroughly investigated, experimentally and theoretically, for its CO_2 capture properties in a variety of CO_2 concentrations and temperatures, and showed excellent isothermal recyclability up to 3 cycles.

Introduction

The global temperature has been increasing for the last 250 years, mostly due to anthropogenic activities that led to extensive greenhouse gas emissions. Those gases are composed of methane (10%), nitrous oxide (5%), fluorinated gases (3%), and, most importantly, carbon dioxide (82%).[1] CO_2 is naturally present in the atmosphere as a part of the biological carbon cycle, but human activities, mainly the combustion of fossil fuels for energy and transportation, are altering this cycle by adding a considerable amount of CO_2 to the atmosphere.[2] This worldwide concern has led nations to unite over the Paris Agreement and collectively propose to lower the greenhouse emissions to keep global warming below 2 °C. To achieve that goal, it is imperative to reduce and mitigate global emissions by the multilateral implementation of climate action plans, which include the development of new technologies to achieve the 2030 Agenda on Sustainable Development.[3] Given this challenge, Carbon Capture and Sequestration (CCS) and Carbon Capture and Utilization (CCU) technologies have been extensively investigated, and the search for more efficient, sustainable, and low-cost CCS and CCU materials remains an ongoing hot topic of research.[4–7]

Among the CCS technologies, aqueous amine solution is vastly used for CO_2 absorption from the flue gas of the coal-fired power plants, which account for over a third of the global electricity generation worldwide. However, its main drawbacks are the strong corrosion of equipment vessels and the high investment costs for industrial implementation. The latter is attributed to the energy-demanding regeneration process, which occurs at temperatures around 100-120 °C and generates a substantial efficiency penalty for the power plants.[8] Due to easier regeneration and substantial uptake capacities, porous materials have been considered powerful candidates for CCS applications. Their chemical robustness, easy pore surface engineering, and thermal stability are key features for improving the tuning of CO_2 adsorption properties.[9,10]

Already known for their gas storage potential,[11–13] Covalent Organic Frameworks (COFs) are porous, crystalline, and fully organic materials.[14] Their chemical tunability, high specific surface area, and thermal stability are important features that allow their application in several fields,[15–18] especially in CO_2 adsorption.[19–21] In this context, Sun *et al.*[22] showed that the N-rich 2D COFs, COF-SDU1, COF-SDU2 and COF-SDU3 exhibited CO_2 uptakes up to 741 mg/g at 25°C and 45 bar. In addition, the authors highlighted that pore size is a key factor for high-pressure adsorption of CO_2. In fact, nitrogen-based COFs prompted interest, since the presence of the CO_2-philic nitrogen allows a Lewis acid-base interaction to take place.[23] Based on that, Jiang *et al.*[24] synthesized a series of imine-linked COFs

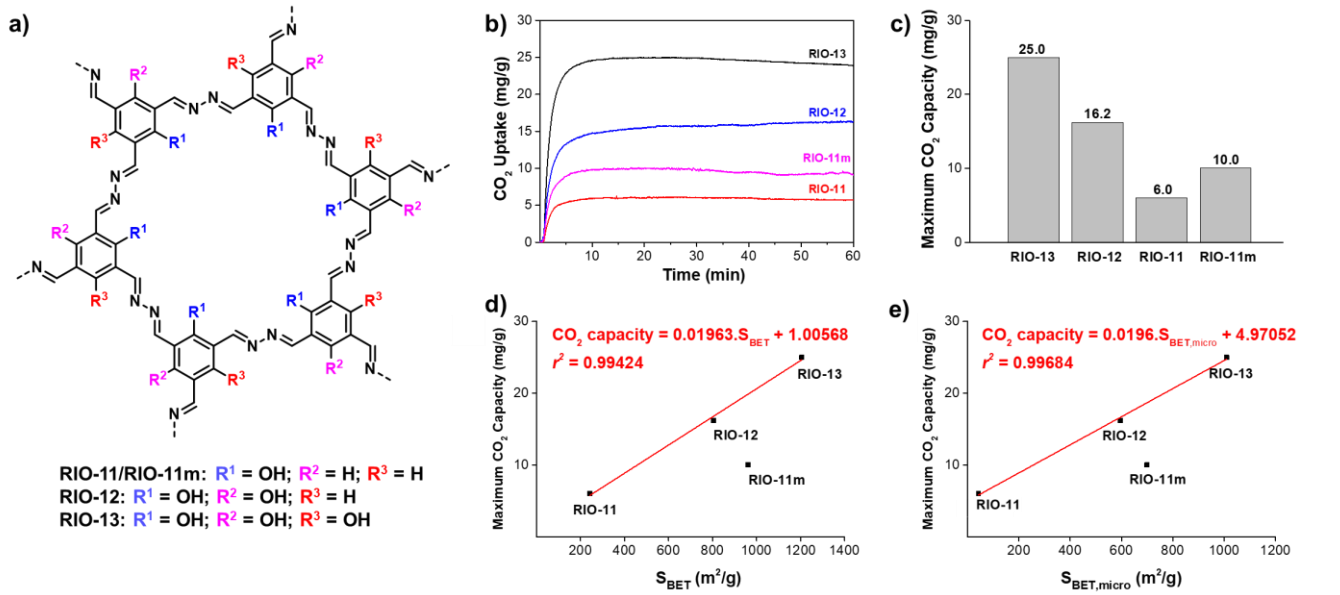

Figure 1. (a) Chemical structure of the COFs RIO-13, RIO,-12, RIO-11, and RIO-11m (synthesized with a modulator); (b) Adsorption isotherms of CO_2 at 40 °C and 1 atm and (c) maximum CO_2 capacity values for RIO-11m, RIO-11, RIO-12, and RIO-13; Plot of the maximum CO_2 uptake capacity versus (d) the total BET specific surface area and (e) the BET micropore specific surface area for RIO-11m, RIO-11, RIO-12, and RIO-13. The linear equations (y = CO_2 capacity; x = S_{BET} or $S_{BET,micro}$) and r^2 values are based solely on RIO-11, RIO-12 and RIO-13.

which were evaluated towards their CO_2 uptake at 1 atm. The nitrogen-based material $[EtNH_2]_{50}$-H_2P-COF presented a CO_2 uptake of 157 mg/g at 0°C, and 82 mg/g at 25°C. Likewise, Mu *et al.*[25] described the microporous azine-based COF-JLU2 synthesized by condensation of hydrazine hydrate and 1,3,5-triformylphloroglucinol. This microporous material displayed a CO_2 uptake up to 217 mg/g at 0°C and 1 bar, besides methane and hydrogen storage capacities as well. The similarly synthesized ATFG-COF, described by Stegbauer *et al.*[26] reached a CO_2 uptake capacity of 173 mg/g at 0°C, 106 mg/g at 25°C, and 82 mg/g at 40°C under 1 bar. Modification of the channels topology by metal-doping to potentially increase the sorption properties did not further enhance the CO_2 uptake for the ATFG-COF.

In this contribution, we investigate the CO_2 uptake capacities for the hydroxy-1,3,5-triformylbenzenes-based COFs, named RIO-13, RIO-12, RIO-11, and RIO-11m.[27] Based on experimental and theoretical studies, this work focuses on improving the understanding of the structure-property relationships between the CO_2 adsorption properties and the material surface and textural features. A deeper focus on the impact of specific surface area and the relative number of hydroxyl groups present in those hydroxybenzene-based COFs was carefully investigated.

Results and Discussion

The microporous 2D COFs RIO-13, RIO-12, RIO-11, and RIO-11m (Figure 1a) were prepared based on the conventional solvothermal synthesis of an imine condensation reaction between hydrazine hydrate and hydroxylated-1,3,5-triformylbenzenes in a mixture of dioxane/mesitylene and an aqueous solution of acetic acid (see Supporting Information for synthetic procedures and characterization details). [27,28] Notably, the COF resulting from 1,3,5-triformylphenol was prepared under two different conditions as its Brunauer-Emmett-Teller (BET) specific surface area and crystallinity are greatly affected by the use (or not) of a modulator in its synthesis. Thus, a lower specific surface area and less crystalline material, RIO-11, is obtained when the conventional solvothermal synthesis is used, and a higher specific surface area material with improved crystallinity, RIO-11m, is obtained when a modulator (aniline) is added to the classical solvothermal method. In contrast, RIO-12 and RIO-13, which show no noticeable changes when a modulator is employed,[27] were only prepared according to the conventional solvothermal procedure. The textural properties of these materials can be found in Table 1.

Table 1. Specific surface area (S_{BET}), micropore specific surface area ($S_{BET,micro}$) obtained by the t-plot method, and pore size of RIO-13, RIO-12, RIO-11, and RIO-11m.

COF	S_{BET} (m^2/g)	$S_{BET,micro}$ (m^2/g)	Pore Size (nm)
RIO-13	1205	1009	1.3
RIO-12	804	595	1.3
RIO-11m	961	699	1.3
RIO-11	242	43	1.3

The materials RIO-13, RIO-12, RIO-11 and RIO-11m were studied by thermogravimetric CO_2 adsorption experiments under flow conditions, at 40 °C and ambient pressure (1 atm), in order to better reproduce post-combustion CO_2 capture conditions.[29–31] By analyzing the CO_2 adsorption isotherms for RIO-11m, RIO-11, RIO-12 and RIO-13 (Figure 1b), it is noticeable that the adsorption capacity of this series follows the order of RIO-13 > RIO-12 > RIO-11m > RIO-11, with maximum CO_2 uptakes values of 25.0 mg/g, 16.2 mg/g, 10.0 mg/g, and 6.0 mg/g, respectively (Figure 1c).

It is worth commenting on the significant differences in the reported maximum CO_2 uptake values when comparing RIO-13 (25 mg/g at 40°C and 1 atm) to COF-JLU2 (217 mg/g at 0°C and 1 bar)[25] and ATGF-COF[26] (82 mg/g at 40 °C and 1 atm). These

differences might indeed be surprising at a first glance since these materials are made from the same building blocks. The reason for these large differences simply results from the fact that the reported maximum adsorption values for COF-JLU2 and ATFG-COF were not obtained under the same thermogravimetric conditions as RIO-13, and therefore cannot be directly compared. However, when ATFG-COF was tested under a thermogravimetric flow, it was reported CO_2 adsorptions up to 66 mg/g at 30 °C and up to 35 mg/g at 50 °C, which are in the range of our findings.

In order to understand the differences in the CO_2 uptake capacities of RIO-11 to RIO-13, we first investigated the CO_2 adsorption in terms of the materials BET specific surface area (S_{BET}), since the latter is reported to have a great impact on the CO_2 adsorption among COF materials.[18,19,22,32] Therefore, the relationship between the CO_2 maximum uptake versus the total S_{BET} and the specific surface area related to the micropores ($S_{BET,micro}$) are presented in Figures 1d,e.

By analyzing both graphs (Figures 1d,e), a linear correlation among RIO-11, RIO-12, and RIO-13 is noticeable, but not for RIO-11m. Indeed, the correlation coefficient calculated for RIO-11, RIO-12, and RIO-13, afforded the r^2-values of 0.9942 and 0.9968 for the S_{BET} and $S_{BET,micro}$, respectively. Thus, there is an overall correlation between the specific surface area and the CO_2 adsorption capacity regarding RIO-11, RIO-12, and RIO-13. However, the specific surface area is obviously not the sole factor that influences the CO_2 adsorption property of these materials, since RIO-11m, in stark contrast, is not a part of this linear relationship. If this was the case, RIO-11m would be expected to have its maximum uptake capacity between RIO-12 and RIO-13. In fact, this can be further explained by the linear coefficient (*b*) from the $y = ax + b$ equation ($y = CO_2$ capacity; $x = S_{BET}$ or $S_{BET,micro}$) in Figures 1d,e. If the specific surface area was indeed the sole responsible for the CO_2 uptake, the *b* coefficient would have to be necessarily zero: no CO_2 capture should occur when the S_{BET} is zero, which is clearly not the case, especially for the $S_{BET,micro}$ relationship (Figure 1e).

Aiming to find a common ground to understand the CO_2 adsorption for these COFs, we next turned our attention to the chemical composition of such materials. Considering that RIO-11m, RIO-11, RIO-12, and RIO-13 bear the same azine backbone and that the major chemical difference among them relies on the degree of hydroxyl groups within the framework (Figure 1a), it seemed reasonable to consider the influence of this functional group regarding their CO_2 adsorption properties. This could justify the difference between the values of experimental and expected results for the maximum CO_2 uptake for RIO-11m, as the relatively lower number of hydroxyl groups in RIO-11m – in comparison to RIO-12 and RIO-13 – may be setting a threshold for its maximum CO_2 capacity. To verify this hypothesis, the CO_2 uptake capacities were converted into their molar basis. In order to perform this conversion, we considered the smallest repetitive unit of the COF as a reference (SRU, Figure 2). Thus, in the hold of the converted uptake values, namely the specific CO_2 uptake (Table 2), this specific relationship was evaluated.

Smallest Repetitive Unit (SRU) of COFs:

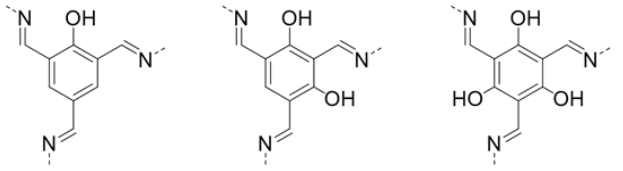

RIO-11/RIO-11m	RIO-12	RIO-13
172.2 g/mol	188.2 g/mol	204.2 g/mol

Figure 2. Smallest Repetitive Unit (SRU) and molar mass (M_{SRU}) of RIO-11, RIO-11m, RIO-12, and RIO-13.

Table 2. Specific CO_2 uptake as a function of the smallest repetitive unit (SRU) of COFs.

COF	M_{SRU} (g/mol)	mmol of SRU *per* 1 g of COF[a]	Max. CO_2 Uptake (mmol/g)[b]	Specific CO_2 Uptake (mmol/mmol)[c]
RIO-13	204.1650	4.898	0.568	0.116
RIO-12	188.1660	5.314	0.368	0.069
RIO-11m	172.1670	5.808	0.227	0.039
RIO-11	172.1670	5.808	0.136	0.023

Determined by [a]: 1 g COF/M_{SRU}; [b] mg CO_2/ CO_2 molar mass; [c] (mmol of captured CO_2)/(mmol of SRU *per* 1 g of COF). For details see supporting information.

Regarding the specific CO_2 uptake capacities, the materials exhibited the following order: RIO-13 > RIO-12 > RIO-11m > RIO-11 (Table 2). Taking RIO-11m as a reference, the CO_2 uptake doubles when the number of hydroxyl groups doubles in RIO-12, and it triplicates when the number of hydroxyl groups triplicates in RIO-13. When RIO-11 is taken as a reference, the CO_2 uptake triplicates for the first case and increases five times for the latter. In both cases, the increase of hydroxyl groups in the chemical structure of the COFs is associated with an increase of the specific CO_2 uptake capacity. Hence, one could consider that an increase in CO_2 adsorption goes along with an increase of the number of hydroxyl groups.

Nevertheless, as RIO-11 and RIO11m both present one hydroxyl group *per* SRU, one could *a priori* expect the same CO_2 affinity for both materials if the number of hydroxyl units would be the sole factor influencing the CO_2 adsorption capacity. In contrast, RIO-11 reaches only 14% of its theoretical S_{BET} value (Table 3),[27] whereas RIO-11m reaches 57%. A possible explanation for the different CO_2 affinity of those materials might be due to defects in their structure which could interfere in gas sorption, the proportion of which would be higher with RIO-11 than RIO-11m. Despite those differences between RIO-11 and RIO-11m, it is here demonstrated that an increase of the hydroxyl groups present in the SRU leads to a unanimous increase of the CO_2 uptake. This is in line with earlier findings from Huang *et al.*, where the porphyrin-based $[EtOH]_X$-H_2P-COFs presented enhanced CO_2 capacities when higher contents of hydroxyl groups were incorporated.[24] Additionally, considering the specific CO_2 uptake capacities of the SRU of

each COF (Table 2) and that each pore is theoretically formed by 6 SRU units (Figure 1a), one can calculate in a first approximation that it takes *ca*. 1.5 pore of a single layer of RIO-13 to capture 1 mmol of CO_2, 2.3 pores of RIO-12, 4.1 pores of RIO-11m, and 7 pores of RIO-11, respectively.

Table 3. Experimental and theoretical S_{BET} of COFs.

COF	$S_{BET,experimental}$ (m^2/g)	$S_{BET,theoretical}$ (m^2/g)[27]	$S_{BET,experimental}$/ $S_{BET,theoretical}$ (%)
RIO-13	1205	1238	97
RIO-12	804	1471	55
RIO-11m	961	1683	57
RIO-11	242	1683	14

The influence of hydroxyl groups on CO_2 capture has been widely reported in the literature for a range of materials with this application.[33–37] The presence of polar groups in conjugated microporous organic polymers was shown to be effective in CO_2 capture.[38] In particular, incorporation of hydroxyl groups would be the main reason for the observed better adsorption, following the tendency of the alike modification in MOF MIL-53 derivatives.[39] Likewise, Férey *et al.*[40] have shown that the very large breathing mode during CO_2 adsorption-desorption experiments for the MOF MIL-53 was partially due to -OH···CO_2 interactions. These interactions were investigated by IR spectroscopy and they were studied based on the significant perturbation of the stretching and the bending modes of the hydroxyl groups upon CO_2 adsorption, which were predicted by periodic DFT calculations. Additionally, according to Schröder *et al.*,[41] hydroxyl groups present within the pore can selectively bind to CO_2 through the formation of moderate -OH···O=C=O hydrogen bonds, as reported for MOF NOTT-300 and detected by in situ PXRD and inelastic neutron scattering studies. In this manner, hydroxyl groups were already demonstrated to act as adsorption sites in porous materials, due to either hydrogen bonds or Lewis acid-base interactions.

To gain a deeper understanding of the structural features of the COFs pore organization and of the CO_2-COFs interactions in the RIO-13-11 series, both a TEM study and a set of DFT calculations were performed. Figure 3 shows HRTEM images of RIO-12 and RIO-13 materials. Individual ball- or flake-like particles of roughly 20 nm have formed in RIO 12, as assessed by the HRTEM image displayed in Figure 3b. Interestingly, it appears that an “octopus-like” crystal growth occurred in both RIO-12 and RIO-13 (Figure 3a,c,d), as observed by Pham-Huu *et al.* for the growth of carbon nanotubes.[42] An extremely organized porous structure arises, probably built by the stacking through non-covalent interactions between individual COF spheres.[43] Haase *et al.*[44] and Wei *et al.*[45] have already observed a unidirectional slip stacking geometry due to the inherent self-complementarity of individual building blocks and the donor-acceptor type stacking of imine groups. One may, therefore, expect a similar unidirectional growth thanks to both azine and hydroxyl groups present in the RIO-12 and RIO-13 frameworks.

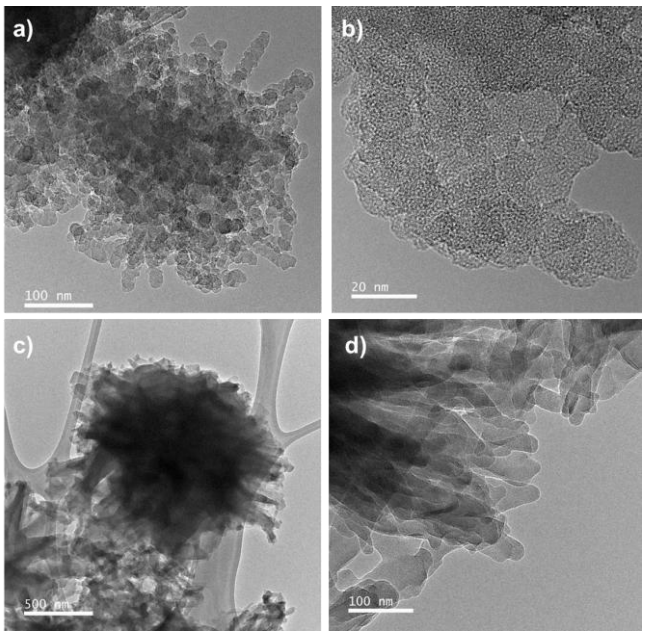

Figure 3. HRTEM images of COF RIO-12 showing (a) an octopus-like crystal growth of (b) a ball-or flake-like nanoparticle morphology. HRTEM images of COF RIO-13 also displaying an octopus-like crystal growth (c,d).

DFT calculations were performed and the equilibrium structures, interaction distances, and adsorption energy found for CO2@COF are presented in Figure 4. It is worth mentioning that RIO-13 presents keto-enol tautomerism.[46,47] Based on experimental NMR data and theoretical calculation, a 1:1 mixture of the keto-enamine and enol-imine tautomeric forms *is the most stable and dominant form* presented by RIO-13 (RIO-$13_{(keto/enol)}$).[47] In contrast, for RIO-12, RIO-11 and RIO-11m, the presence of tautomers was not evidenced by the ^{13}C CP-MAS NMR spectroscopy, as the iminol form was the only one detected (Figures S2 and S3). Of note, calculations were also performed for a COF without any hydroxyl group, named RIO-10, in order to fully access the influence that -OH groups may have on the adsorption phenomenon.

Based on those calculations, it is possible to distinguish clear differences among the adsorption energy in RIO-10, RIO-11, RIO-12, and RIO-13. For RIO-11 and RIO-12, the calculation results showed that the CO_2 molecule can interact with the lone electron pair of both heteroatoms in the COF framework: *(i)* the oxygen atom from the hydroxyl group and *(ii)* the nitrogen atom from the imine group. Interestingly, the adsorption on the hydroxyl group is energetically favored in both cases. Conversely, for RIO-13, only the lone electron pair of the oxygen atom is available for interaction with the CO_2 molecule, as the hydrogen bond formed with the nitrogen atom prevents access to this interaction site.

For RIO-10, the sole CO_2 interaction with the lone electron pair from the nitrogen of the imine bond resulted in a minimum on the potential energy surface. The adsorption energy is 17.9 kJ/mol with an equilibrium distance of 3.813 Å. This large interaction distance can be attributed to the steric hindrance due to the hydrogen atoms of the neighboring groups to the nitrogen atom.

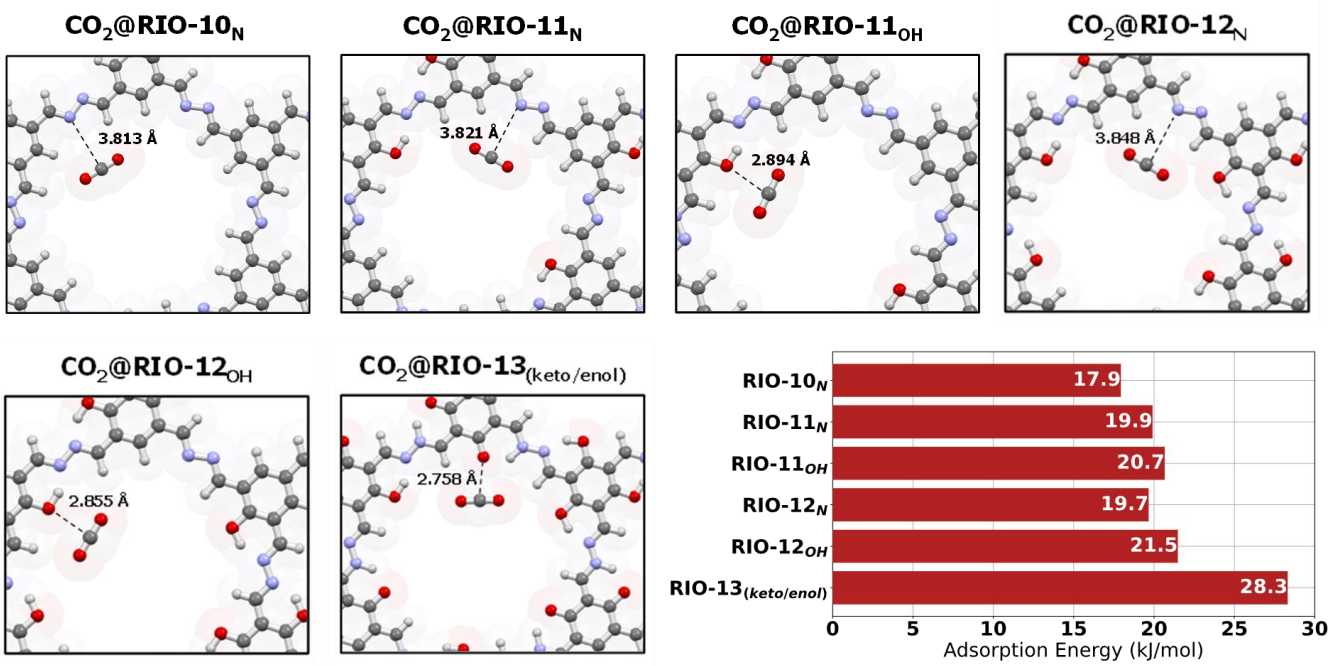

Figure 4. Equilibrium structure of CO_2 adsorbed on RIO-10, -11, -12, and -13 structures. For RIO-11 and RIO-12 two different adsorption sites were explored and for RIO-13 the enol-imine, keto-enamine, and a 1:1 mixture of keto-enamine and enol-imine tautomeric forms were considered.

For RIO-11, the CO_2 adsorption energy is 19.9 kJ/mol for the nitrogen atom (CO_2@RIO-11_N) and 20.7 kJ/mol for the oxygen atom (CO_2@RIO-11_{OH}). For this system, the equilibrium distance between the CO_2 and the adsorption site 3.821 Å for the nitrogen atom and 2.894 Å for the oxygen atom. RIO-12 showed slightly higher adsorption energy: 19.7 kJ/mol for adsorption of CO_2 on the nitrogen atom (CO2@RIO-12_N) and 21.5 kJ/mol for the adsorption on the -OH sites (CO_2@RIO-12_{OH}). The equilibrium distances of 3.848 Å and 2.855 Å were found for the N and -OH sites, respectively. The interaction distance between CO_2 and the nitrogen atom for RIO-11 and RIO-12 is thus roughly the same as that presented by RIO-10. However, the interaction energy is *ca.* 2 kJ/mol higher, indicating that the presence of -OH groups can help stabilize the adsorption phenomenon, even when it occurs on the N atom.

For RIO-13 the 1:1 mixture of the keto/enol tautomers (CO_2@RIO-$13_{keto/enol}$) presented CO_2 electronic adsorption energy of 28.3 kJ/mol on the oxygen atom, and a $C_{CO2}\cdots O_{COF}$ equilibrium distance of 2.758 Å. Thus, since the overall adsorption energies on the oxygen atoms are higher than the adsorption energy on the nitrogen atoms, it is possible to conclude that the substantial increase in CO_2 adsorption on RIO-13, when compared to RIO-10, is strongly related to its higher number of hydroxyl groups within the pore. In addition, the 1: 1 mixture of the tautomeric forms (CO2@RIO-$13_{keto/enol}$) showed a highest adsorption energy than the pure tautomeric forms – RIO-13_{enol} or RIO-13_{keto} - which showed adsorption energies of 20.9 and 26.4 kJ/mol, respectively.

Hence, the theoretical calculations corroborate that the CO_2 adsorption capacities of RIO-13 > RIO-12 > RIO-11/RIO-11m are based on the preferential adsorption sites, which agrees with our experimental findings. In addition, this CO_2 affinity for the hydroxyl groups could justify that even though RIO-11m presents a higher specific surface area than RIO-12, its CO_2 adsorption capacity is impaired by the lack of CO_2-active binding sites. Indeed, the presence of limited hydroxyl groups seems to act as a threshold of CO_2 uptake, which leads to a smaller CO_2 uptake capacity of RIO-11 and RIO-11m in comparison to RIO-12 or RIO-13.

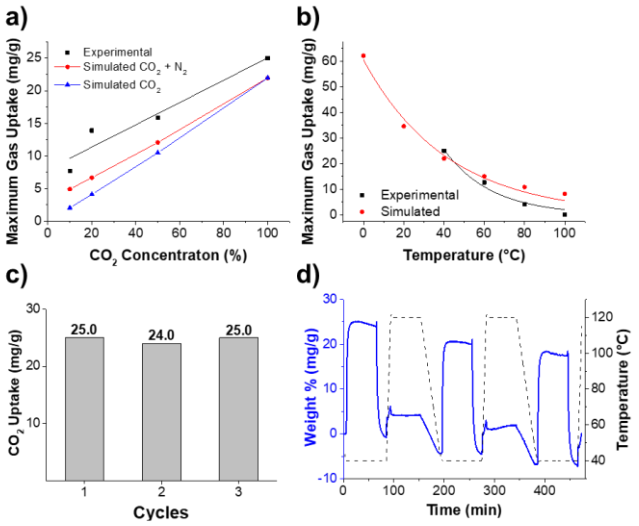

Figure 5. (a) Plot of CO_2 concentration versus the maximum gas capacity and (b) plot of adsorption temperature versus the maximum gas capacity, both for RIO-13. (c,d) Recyclability test for CO_2 adsorption for COF RIO-13 at 40 °C and 1 atm.

Aiming to further explore our best performing CO_2-philic material RIO-13 towards CCS application, the study of other adsorption conditions, namely the CO_2 adsorption temperature and gas concentration, were investigated both experimentally and theoretically. Considering the CO_2 composition, different concentrations of the gas were investigated: 100%, 50%, 20%, and 10% of CO_2 in N_2. RIO-13 presented maximum gas uptake capacities of 25.0 mg/g, 15.9 mg/g, 13.9 mg/g, and 7.7 mg/g, respectively (Figure 5a). To elucidate the adsorption selectivity

of these gases, Grand-Canonical Monte Carlo simulations were performed under the same conditions of pressure, temperature and concentration. At a CO_2 concentration of 10%, the molar ratio of adsorbed CO_2/N_2 is 0.46. This value increases to 1.02 at a CO_2 concentration of 20%, and to 4.25 at a CO_2 concentration of 50%, thus indicating a higher selectivity for CO_2 than for N_2 when the CO_2 concentration is greater than 10%. Figure 5a shows additionally the result of the simulations for the total gas uptake (CO_2 + N_2) and for solely the CO_2 uptake at different concentrations.

The CO_2 adsorption temperature was varied to further characterize the sorption properties of our best CO_2 capture material RIO-13. The temperatures investigated were 40 °C, 60 °C, 80 °C and 100 °C (Figure 5b). When the experiment was performed at 40 °C, the maximum experimental adsorption uptake of 25.0 mg/g was observed. When the adsorption temperatures were 60 °C and 80 °C, the maximum CO_2 uptakes were 12.6 mg/g and 4.0 mg/g, respectively. No relevant adsorption was observed when the temperature was 100 °C. Therefore, the CO_2 adsorption capacity increases with a decrease in the temperature for RIO-13. As it happens for most physisorption cases,[25,48,49] a lower adsorption temperature leads to a higher CO_2 uptake due to less kinetic energy attributed to the adsorbed gas. This difference in energy indeed makes it is less probable that the gas escapes the material surface at a lower temperature, especially when physisorption takes place.

Finally, aiming to access the recyclability of this COF, three adsorption-desorption cycles were performed to evaluate the recyclability of RIO-13 (Figures 6c,d). Interestingly, no additional heat was necessary to desorb the CO_2, which was simply liberated from the COF surface, isothermally at 40 °C, when the CO_2 flow was replaced by N_2. After 3 cycles, the material exhibited no significant loss in CO_2 uptake and demonstrated easy regeneration. This characteristic is attributed to soft binding interactions between the RIO-13 and CO_2 molecules, which are responsible for fully reversible isotherms in an “easy-on/easy-off” system.[41] This regeneration feature needs to be highlighted, as most materials require temperature swing adsorption (TSA), vacuum swing adsorption (VSA), or pressure swing adsorption (PSA) processes to be fully regenerated.[50] Additionally, the no-heat recovery of RIO-13 is another significant feature,[51] especially when compared with the costly thermal regeneration of current amine-based CCS materials.

Conclusion

This study presents the experimental and theoretical study of the CO_2 adsorption properties of the microporous COFs, RIO-11m, RIO-11, RIO-12, and RIO-13 employing post-combustion conditions: 1 atm, and 40 °C. Although the BET specific surface area is relevant for the CO_2 adsorption properties of these materials, it was shown, experimentally and theoretically, that the relative number of hydroxyl groups acts as a threshold for their uptake capacities, mainly due to their preferential binding sites to carbon dioxide due to Lewis acid-base interactions. As the best result for the series, RIO-13 demonstrated good CO_2 uptakes for a 100% CO_2 flow, enhanced by lower temperatures. Finally, its isothermal regeneration up to 3 cycles is of high importance, since no TSA, VSA, or PSA processes were needed to fully recover the material to its initial adsorption capacities. As in practical situations water is likely to be present, it would be of interest to study the stability of those materials under humid conditions, along with their selective CO_2 capture in this media. Finally, we expect to contribute to a further understanding of the COF structure-CO_2 adsorption relationship, and to the development of new -OH decorated COFs based on their CO_2-philic properties.

Experimental Section

Instruments and methods

TEM images were acquired after the dispersion of the samples in ethanol, sonication for a few seconds, and drop-deposition on a copper grid with a holey carbon film. HRTEM images were acquired over a Hitachi HF-3300kV instrument. Thermogravimetric CO_2 adsorption-desorption experiments at 1 atm were performed in a TGA Q50 TA Instrument. Firstly, the samples were submitted to 1 h heating at 120 °C under N_2 flow to clean their surfaces. Then, the samples were cooled down until the desired temperature, where samples were isothermally exposed to a CO_2 flow of 30 mL/min. The hold time for CO_2 adsorption was 60 min, even though complete saturation of the surface occurred before 10 min. After this step, the gas flow was switched to N_2 under the same temperature for 10-20 min. Samples were finally heated to 120 °C under N_2 flow and additional adsorption experiments using different concentrations of 10%, 20%, 50%, and 100% of CO_2 in N_2 were performed. The recyclability test was performed under a 100% CO_2 flow at 40 °C.

Computational details

DFT calculations under periodic boundary conditions were performed using Quantum ESPRESSO code version 6.2.4.[52,53] The electron-ion interactions were described by ultrasoft RRKJ pseudopotentials[54] and the exchange and correlation effects were treated with a GGA-PBE[55] functional. The Kohn-Sham orbitals were expanded on a plane-wave basis set with a kinetic-energy cutoff of 80 Ry, charge density cutoff of 600 Ry, and the first Brillouin Zone integrations were performed on a Γ-centered 6x6x12 Monkhorst-Pack[56] k-points mesh. The D3 correction method proposed by Grimme *et al.*[57] was used to treat the van der Waals interactions. The CO_2@COF adsorption electronic energy ($\mathbf{\Delta E^{el}_{ads}}$) was calculated as the difference between the electronic energy of the interacting system ($\mathbf{E_{CO2@COF}}$) and the isolated CO_2 ($\mathbf{E_{CO2}}$) and COFs ($\mathbf{E_{COF}}$):

$$\mathbf{\Delta E^{el}_{ads} = E_{CO2@COF} - E_{CO2} - E_{COF}}$$

Force field-based Grand-Canonical Monte Carlo (GCMC) simulations were performed based on the RASPA[58] package. For all GCMC simulations, 10000 initiation cycles and 50000 running cycles were employed in a 2x2x7 supercell. A Lennard-Jones potential with parameters taken from the TraPPE[59] force field was used to treat the van der Waals interactions of adsorbed molecules (N_2 and CO_2).

Acknowledgements

This study was financed by the Coordenação de Aperfeiçoamento de Pessoal de Nível Superior – Brasil (CAPES) – Finance Code 001; CAPES scholarship PDSE Process Number 88881.189512/2018-01, China-France Cai Yuanpei Grant and CNPq. The authors acknowledge the Núcleo Avançado de Computação de Alto Desempenho (NACAD) of

COPPE/UFRJ for the computational facility and the Cai Yuanpei program between France-China. We thank Dr.Sangaraju Shanmugam (Daegu Gyeongbuk Institute of Science and Technology—DGIST) for performing the HRTEM analysis. V.R. thanks the Institut Universitaire de France for financial support. The authors declare no conflict of interest.

Keywords: Covalent Organic Frameworks • CO_2 Capture • DFT calculations • Hydroxyl-CO_2 interaction • structure-CO_2 adsorption relationship

[1] "Global Greenhouse Gas Emissions Data by the United States Environmental Protection Agency - EPA." Can be found under https://www.epa.gov/ghgemissions/global-greenhouse-gas-emissions-data, (accessed Oct 1st, 2019).
[2] T. J. Battin, S. Luyssaert, L. A. Kaplan, A. K. Aufdenkampe, A. Richter, L. J. Tranvik, *Nat. Geosci.* **2009**, *2*, 598–600.
[3] **2016**.
[4] K. Riahi, E. S. Rubin, M. R. Taylor, L. Schrattenholzer, D. Hounshell, *Energy Econ.* **2004**, *26*, 539–564.
[5] A. A. Olajire, *Energy* **2010**, *35*, 2610–2628.
[6] M. K. Mondal, H. K. Balsora, P. Varshney, *Energy* **2012**, *46*, 431–441.
[7] K. S. Lackner, *Science* **2003**, *300*, 1677–1678.
[8] K. Goto, K. Yogo, T. Higashii, *Appl. Energy* **2013**, *111*, 710–720.
[9] C. Megías-Sayago, R. Bingre, L. Huang, G. Lutzweiler, Q. Wang, B. Louis, *Front. Chem.* **2019**, *7*, 1–10.
[10] S. Zhang, Q. Wang, P. Puthiaraj, W.-S. Ahn, *J. CO_2 Util.* **2019**, *34*, 395–403.
[11] M. G. Rabbani, A. K. Sekizkardes, Z. Kahveci, T. E. Reich, R. Ding, H. M. El-Kaderi, *Chem. Eur. J.* **2013**, *19*, 3324–3328.
[12] S. S. Han, H. Furukawa, O. M. Yaghi, W. A. Goddard, *J. Am. Chem. Soc.* **2008**, *130*, 11580–11581.
[13] Z. Li, X. Feng, Y. Zou, Y. Zhang, H. Xia, X. Liu, Y. Mu, *Chem. Commun.* **2014**, *50*, 13825–13828.
[14] A. P. Côte, A. I. Benin, N. W. Ockwig, M. O'Keeffe, A. J. Matzger, O. M. Yaghi, *Science* **2005**, *310*, 1166–1170.
[15] X. Feng, X. Ding, D. Jiang, *Chem. Soc. Rev.* **2012**, *41*, 6010.
[16] S.-Y. Ding, W. Wang, *Chem. Soc. Rev.* **2013**, *42*, 548–568.
[17] P. J. Waller, F. Gándara, O. M. Yaghi, *Acc. Chem. Res.* **2015**, *48*, 3053–3063.
[18] H. Furukawa, O. M. Yaghi, *J. Am. Chem. Soc.* **2009**, *131*, 8875–8883.
[19] Y. Zeng, R. Zou, Y. Zhao, *Adv. Mater.* **2016**, *28*, 2855–2873.
[20] J. Ozdemir, I. Mosleh, M. Abolhassani, L. F. Greenlee, R. R. Beitle, M. H. Beyzavi, *Front. Energy Res.* **2019**, *7*, 77.
[21] A. A. Olajire, *J. CO_2 Util.* **2017**, *17*, 137–161.
[22] M. Zhang, R. Zheng, Y. Ma, R. Chen, X. Sun, X. Sun, *Microporous Mesoporous Mater.* **2019**, *285*, 70–79.
[23] G. Sethia, A. Sayari, *Carbon N. Y.* **2015**, *93*, 68–80.
[24] N. Huang, R. Krishna, D. Jiang, *J. Am. Chem. Soc.* **2015**, *137*, 7079–7082.
[25] R. Xue, H. Guo, T. Wang, L. Gong, Y. Wang, J. Ai, D. Huang, H. Chen, W. Yang, *Anal. Methods* **2017**, *9*, 3737–3750.
[26] L. Stegbauer, M. W. Hahn, A. Jentys, G. Savasci, C. Ochsenfeld, J. A. Lercher, B. V. Lotsch, *Chem. Mater.* **2015**, *27*, 7874–7881.
[27] R. A. Maia, F. L. Oliveira, M. Nazarkovsky, P. M. Esteves, *Cryst. Growth Des.* **2018**, *18*, 5682–5689.
[28] R. A. Maia, F. Berg, V. Ritleng, B. Louis, P. M. Esteves, *Chem. Eur. J.* **2020**, *26*, 2051–2059.
[29] A. Alonso, J. Moral-Vico, A. Abo Markeb, M. Busquets-Fité, D. Komilis, V. Puntes, A. Sánchez, X. Font, *Sci. Total Environ.* **2017**, *595*, 51–62.
[30] H. Li, K. Wang, Y. Sun, C. T. Lollar, J. Li, H. C. Zhou, *Mater. Today* **2018**, *21*, 108–121.
[31] X. Ge, S. Ma, in *Mater. Carbon Capture*, Wiley, **2020**, pp. 5–27.
[32] S. Zhao, B. Dong, R. Ge, C. Wang, X. Song, W. Ma, Y. Wang, C. Hao, X. Guo, Y. Gao, *RSC Adv.* **2016**, *6*, 38774–38781.
[33] A. Danon, P. C. Stair, E. Weitz, *J. Phys. Chem. C* **2011**, *115*, 11540–11549.
[34] M. Cabrejas Manchado, J. M. Guil, A. Perez Masia, A. Ruiz Paniego, J. M. Trejo Menayo, *Langmuir* **1994**, *10*, 685–691.
[35] C. E. Nanayakkara, W. A. Larish, V. H. Grassian, *J. Phys. Chem. C* **2014**, *118*, 23011–23021.
[36] J. K. You, H. Park, S. H. Yang, W. H. Hong, W. Shin, J. K. Kang, K. B. Yi, J.-N. Kim, *J. Phys. Chem. B* **2008**, *112*, 4323–4328.
[37] M. B. Yue, L. B. Sun, Y. Cao, Z. J. Wang, Y. Wang, Q. Yu, J. H. Zhu, *Microporous Mesoporous Mater.* **2008**, *114*, 74–81.
[38] R. Dawson, D. J. Adams, A. I. Cooper, *Chem. Sci.* **2011**, *2*, 1173.
[39] A. Torrisi, R. G. Bell, C. Mellot-Draznieks, *Cryst. Growth Des.* **2010**, *10*, 2839–2841.
[40] C. Serre, S. Bourrelly, A. Vimont, N. A. Ramsahye, G. Maurin, P. L. Llewellyn, M. Daturi, Y. Filinchuk, O. Leynaud, P. Barnes, G. Férey, *Adv. Mater.* **2007**, *19*, 2246–2251.
[41] S. Yang, J. Sun, A. J. Ramirez-Cuesta, S. K. Callear, W. I. F. David, D. P. Anderson, R. Newby, A. J. Blake, J. E. Parker, C. C. Tang, M. Schröder, *Nat. Chem.* **2012**, *4*, 887–894.
[42] C. Pham-Huu, R. Vieira, B. Louis, A. Carvalho, J. Amadou, T. Dintzer, M. J. Ledoux, *J. Catal.* **2006**, *240*, 194–202.
[43] S. Wang, Z. Zhang, H. Zhang, A. G. Rajan, N. Xu, Y. Yang, Y. Zeng, P. Liu, X. Zhang, Q. Mao, Y. He, J. Zhao, B.-G. Li, M. S. Strano, W.-J. Wang, *Matter* **2019**, *1*, 1592–1605.
[44] F. Haase, K. Gottschling, L. Stegbauer, L. S. Germann, R. Gutzler, V. Duppel, V. S. Vyas, K. Kern, R. E. Dinnebier, B. V. Lotsch, *Mater. Chem. Front.* **2017**, *1*, 1354–1361.
[45] H. Wei, S. Chai, N. Hu, Z. Yang, L. Wei, L. Wang, *Chem. Commun.* **2015**, *51*, 12178–12181.
[46] S. Jhulki, A. M. Evans, X.-L. Hao, M. W. Cooper, C. H. Feriante, J. Leisen, H. Li, D. Lam, M. C. Hersam, S. Barlow, J.-L. Brédas, W. R. Dichtel, S. R. Marder, *J. Am. Chem. Soc.* **2020**, *142*, 783–791.
[47] L. Stegbauer, M. W. Hahn, A. Jentys, G. Savasci, C. Ochsenfeld, J. A. Lercher, B. V. Lotsch, *Chem. Mater.* **2015**, *27*, 7874–7881.
[48] R. Gomes, P. Bhanja, A. Bhaumik, *Chem. Commun.* **2015**, *51*, 10050–10053.
[49] H. A. Patel, S. H. Je, J. Park, Y. Jung, A. Coskun, C. T. Yavuz, *Chem. Eur. J.* **2014**, *20*, 772–780.
[50] J. A. Mason, K. Sumida, Z. R. Herm, R. Krishna, J. R. Long, *Energy Environ. Sci.* **2011**, *4*, 3030.
[51] R. S. Haszeldine, *Science* **2009**, *325*, 1647–1652.
[52] P. Giannozzi, S. Baroni, N. Bonini, M. Calandra, R. Car, C. Cavazzoni, D. Ceresoli, G. L. Chiarotti, M. Cococcioni, I. Dabo, A. Dal Corso, S. de Gironcoli, S. Fabris, G. Fratesi, R. Gebauer, U. Gerstmann, C. Gougoussis, A. Kokalj, M. Lazzeri, L. Martin-Samos, N. Marzari, F. Mauri, R. Mazzarello, S. Paolini, A. Pasquarello, L. Paulatto, C. Sbraccia, S. Scandolo, G. Sclauzero, A. P. Seitsonen, A. Smogunov, P. Umari, R. M. Wentzcovitch, *J. Phys. Condens. Matter* **2009**, *21*, 395502.
[53] P. Giannozzi, O. Andreussi, T. Brumme, O. Bunau, M. Buongiorno Nardelli, M. Calandra, R. Car, C. Cavazzoni, D. Ceresoli, M. Cococcioni, N. Colonna, I. Carnimeo, A. Dal Corso, S. de Gironcoli, P. Delugas, R. A. DiStasio, A. Ferretti, A. Floris, G. Fratesi, G. Fugallo, R. Gebauer, U. Gerstmann, F. Giustino, T. Gorni, J. Jia, M. Kawamura, H.-Y. Ko, A. Kokalj, E. Küçükbenli, M. Lazzeri, M. Marsili, N. Marzari, F. Mauri, N. L. Nguyen, H.-V. Nguyen, A. Otero-de-la-Roza, L. Paulatto, S. Poncé, D. Rocca, R. Sabatini, B. Santra, M. Schlipf, A. P. Seitsonen, A. Smogunov, I. Timrov, T. Thonhauser, P. Umari, N. Vast, X. Wu, S. Baroni, *J. Phys. Condens. Matter* **2017**, *29*, 465901.
[54] A. M. Rappe, K. M. Rabe, E. Kaxiras, J. D. Joannopoulos, *Phys. Rev. B* **1990**, *41*, 1227–1230.
[55] J. P. Perdew, K. Burke, M. Ernzerhof, *Phys. Rev. Lett.* **1996**, *77*, 3865–3868.
[56] H. J. Monkhorst, J. D. Pack, *Phys. Rev. B* **1976**, *13*, 5188–5192.
[57] S. Grimme, J. Antony, S. Ehrlich, H. Krieg, *J. Chem. Phys.* **2010**, *132*, 154104.
[58] D. Dubbeldam, S. Calero, D. E. Ellis, R. Q. Snurr, *Mol. Simul.* **2016**, *42*, 81–101.
[59] J. J. Potoff, J. I. Siepmann, *AIChE J.* **2001**, *47*, 1676–1682.

Covalent Organic Frameworks were investigated towards their CO_2 capture properties as a function of their textural and chemical features. Experimental and theoretical data indicated that the relative number of hydroxyl groups in the COF backbone acts as an adsorption threshold. For the best performing COF, a variety of CO_2 concentrations and temperatures were investigated, showing excellent isothermal recyclability up to 3 cycles.

Institute and/or researcher Twitter usernames: @ufrj @unistra @InstUnivFr @pierreesteves @FeliipeLopess